






Original Article


Multiscale characteristics of the wetting deformation of Malan loess in the Yan'an area, China

NAN Jing-jing^{1,2}  <https://orcid.org/0000-0003-0483-0207>; e-mail: 2016026031@chd.edu.cn

PENG Jian-bing^{1,2} *  <https://orcid.org/0000-0003-4689-7717>;  e-mail: dicexy_1@126.com

ZHU Feng-ji³  <https://orcid.org/0000-0002-3891-5447>; e-mail: zhufj@jk.com.cn

ZHAO Jun-yan^{1,2}  <https://orcid.org/0000-0002-2571-6529>; e-mail: 2019026039@chd.edu.cn;

LENG Yan-qiu^{1,2}  <https://orcid.org/0000-0002-7934-6113>; e-mail: lengyanqiu@chd.edu.cn

* Corresponding author

¹ Department of Geological Engineering, Chang'an University, Xi'an 710054, China

² Key Laboratory of Western China Mineral Resources and Geological Engineering, Ministry of Education, Xi'an 710054, China

³ China JIKAN Research Institute of Engineering Investigations and Design Co., Ltd., Xi'an 710043, China

Citation: Nan JJ, Peng JB, Zhu FJ, et al. (2021) Multiscale characteristics of the wetting deformation of Malan loess in the Yan'an area, China. *Journal of Mountain Science* 18(4). <https://doi.org/10.1007/s11629-020-6490-8>

© Science Press, Institute of Mountain Hazards and Environment, CAS and Springer-Verlag GmbH Germany, part of Springer Nature 2021

Abstract: Loess is prone to collapse upon wetting due to its open metastable structure, which poses a considerable threat to the environment, construction processes and human life. In this study, double oedometer tests and scanning electron microscopy and mercury intrusion porosimetry analyses were conducted on loess from Yan'an to study the macroscopic and microscopic characteristics of loess wetting deformation and the underlying mechanism. The wetting collapse of loess under loading depends on the changes in different microstructure levels and elements. This collapse chain reaction is manifested by the dissipation, scattering and recombination of the cementation, deformation and reorganization of the particles, blocking of the pore channels, decrease in the dominant size and volume of unstable macropores (>14 μm) and abundant mesopores (2.5–14 μm), increase in the volume of small pores (0.05–2.5 μm), and volume contraction at the macroscale. This process is dependent on the initial water content,

stress level and wetting degree. These findings can facilitate collapsible loess hazard prevention and geological engineering construction.

Keywords: Loess; Macroscopic wetting deformation; Wetting collapse mechanism; Microstructure; Pore change

1 Introduction

Loess is a regional soil deposited under arid and semiarid conditions and is widely distributed in Asia, Europe, Africa, North America and South America (Derbyshire and Mellors 1988; Rogers et al. 1994; Muñoz-Castelblanco et al. 2011; Giménez et al. 2012; Milodowski et al. 2015). The Loess Plateau in Northwest China, covering approximately 324,600 km² (Peng et al. 2019), hosts the most characteristic of loess deposits observed. The deep loess strata record the complete 2.4-million-year evolution of the natural

Received: 25-Sep-2020

Revised: 14-Dec-2020

Accepted: 05-Feb-2021

environment, climate and surface geological hazards (Peng et al. 2014). Due to the complex geological structure (strong uplift, diverse landforms, fragmented topography and unique stratigraphic units), variable climate (dry climate, concentrated rainfall and extreme weather) and impact of human activities (agricultural irrigation and construction projects) (Yan et al. 2019), geological hazards such as foundation subsidence, ground fissures, landslides, landslides and debris flows occur frequently in the loess regions of the Loess Plateau (Xu et al. 2012; Zhu et al. 2017; Cui et al. 2018; Zhang et al. 2019a; Peng et al. 2019; Wang et al. 2020b), accounting for approximately one-third of the total number of geological hazards that occur in China every year (Peng et al. 2014). Therefore, the unique mechanical behavior and engineering properties of loess and its catastrophic effect have become research topics of increased interest. As a major engineering and building material in loess regions, loess is generally in unsaturated state and susceptible to collapse upon wetting and loading (Shao et al. 2018; Zhao et al. 2019; Li et al. 2019a). The collapsibility of loess and its subsequent collapse hazards (such as differential settlement, collapse cracks and pits, and slope instability) pose a considerable threat to the environment, construction and human life in this area (Xu et al. 2012; Leng et al. 2018; Zhang et al. 2019b). To handle engineering geology problems associated with the collapse of natural loess, it is essential to study loess collapsibility and its underlying mechanism.

In previous studies, the collapsibility of loess has commonly been evaluated by its maximum collapsibility potential (settlement) under a saturated water content and loading in previous studies (Gao and Gao 1980; Lei 1988; Lin 1995; Nouaouria et al. 2008; Li et al. 2019b). However, in practical engineering, loess is often moistened to a certain water content under surface water seepage or rising groundwater (Shao et al. 2018), and the soil will undergo significant volume changes (Zhao et al. 2019) when it is not fully saturated. Therefore, it is of practical significance to study the unsaturated collapsibility (wetting collapse) of loess wetted to different water contents. Chen et al. (2006) conducted compression tests on intact loess from Xi'an to reveal the variation of wetting deformation characteristics of loess with increasing water content and pressure and its internal relation to the loess structure. Jiang et al. (2012) investigated the effect of different water content increments on the collapse deformation of

artificial structural loess under different stress levels using triaxial wetting tests. Xing et al. (2019) performed oedometer tests on unsaturated loess from Ili to investigate the variation in wetting deformation with increasing moistening level under various vertical stresses. In this study, double oedometer tests were conducted on natural loess with various initial water contents from Yan'an to investigate the whole process of wetting deformation from an unsaturated state to a saturated condition under different vertical pressures with respect to a critical void ratio.

Several traditional approaches have been proposed to interpret the collapsibility mechanism of loess, which has been interpreted as the loss of capillary tension (Alfi 1984), influence of soluble salt solutions (Houston et al. 1988), limited amount of colloidal clay (Rogers et al. 1994), occurrence of water-film wedge action, and consequence of under compaction (Houston et al. 1988; Tadealli and Fredlund 1991). Although these hypotheses and theories have their own bases and help to better understand collapsible loess soils (Zhang et al. 2019b), they only consider unilateral factors (from physical, chemical or geological perspectives). The microstructure (structural theory), including particles, cementation bonds, contact relations and pores, can interpret the nature of loess collapsibility (Barden et al. 1973; Derbyshire and Mellors 1988; Assallay et al. 1997; Romero and Simms 2008). Loess is a special geological body prone to hazards; due to its specific provenance and sedimentary environment, loess has a natural fabric with a high porosity and weak cementation and incomplete consolidation (Peng et al. 2014). The structural damage and destruction of loess under external environmental changes leads to loess compression, collapse and other macroscopic deformation and failure phenomena, thus forming various geological hazards. Therefore, multiscale research combining the wetting deformation and microstructure variations in loess under external action is of great significance for revealing its failure mechanism and catastrophic effects.

Advanced techniques and methods including scanning electron microscopy (SEM), mercury intrusion porosimetry (MIP), X-ray diffraction (XRD), computed tomography (CT) and nuclear magnetic resonance (NMR) are very useful for understanding the microstructure of loess (Gao and Gao 1980; Ng et al. 2017; Wei et al. 2019; Cheng et al. 2020) and its relationship to wetting deformation (Lei 1988; Jiang

et al. 2014a; Li et al. 2019b). Rogers et al. (1994) and Giménez et al. (2012) showed that soil collapse mainly occurs due to particle packing. Muñoz-Castelblanco et al. (2011) explained that the compression of natural loess with a low constant water content is related to the collapse of the largest dry pores. Liu et al. (2016) proposed a conceptual microstructural model with a four-tiered hierarchy to represent the structural characteristics of loess and to illustrate its high collapsibility. Shao et al. (2018) used SEM and MIP to investigate the collapse characteristics and microstructural alteration of remolded loess under graded wetting tests. These researchers suggested that a reduction in the inter-aggregate pore size is the main factor for the collapsibility of remolded loess. Li et al. (2019a) found that in collapse tests, inter-aggregate pores transform into intra-aggregate pores, and the total number of pores increases; the pores become flatter but remain randomly orientated. Wang et al. (2020a) showed that the inundating-induced change in pore size distribution is influenced by loading conditions and that both large pores and medium pores collapse upon inundating under sufficient vertical stresses. Zhang et al. (2019b) carried out environmental scanning electron microscopy (ESEM) tests to observe the specific movement and changes in particles in the same area and found that intergranular cement would change cyclically during multiple humidification processes. Mu et al. (2020) revealed that only the inter-aggregate pores in both saturated intact and compacted loess decrease during isotropic compression. Wei et al. (2020) performed CT, XRD and SEM tests to interpret the 3D microstructural evolution during collapse and the loess collapsibility mechanism. However, there is still limited knowledge and little experimental evidence of the relationship between the macro- and micro characteristics of loess wetting deformation under complicated stress paths. Characterizing the changes in the microstructure system, especially the pore characteristics (pore volume, pore size distribution, pore fractal classification, characteristic pore diameters, etc.), during wetting deformation is valuable for understanding the underlying mechanism of loess wetting collapse. This characterization could provide a scientific reference and quantitative parameters for developing multiscale constitutive models (numerical models) considering microstructural characteristics to better simulate the mechanical behavior of loess

under multifactor coupling (Jiang et al. 2014a; Li et al. 2018; Wei et al. 2019; Li et al. 2019b).

Therefore, in this study, the macroscopic characteristics of wetting deformation (compression, collapsibility and wetting collapse) of natural loess with various initial water contents from Yan'an city, China, were investigated by oedometer tests. SEM and MIP tests were performed on the loess samples before and after the oedometer tests at different stress levels to study the microstructural characteristics and their relationship with the wetting deformation. The results are expected to contribute to improving the interpretation of the wetting collapse of loess under loading and the mechanism behind this behavior from a microscopic perspective, thereby preventing loess collapse hazards and facilitating geological engineering construction.

2 Materials and Methods

2.1 Soil sample characterization

The loess samples were obtained from the excavation area of the major land-creation project in the Yan'an, central Loess Plateau of China (Fig. 1a and b). The soil profile of the sampling site consists of two main stratigraphical units: Q_3 (Malan) loess and Q_2 (Lishi) loess underlying Q_3 loess (over 30 m thick) (Fig. 1c). The soil samples were collected at a depth of 5 m below the surface and correspond to Malan loess (Fig. 1d). Malan loess is a highly porous, clastic, brittle

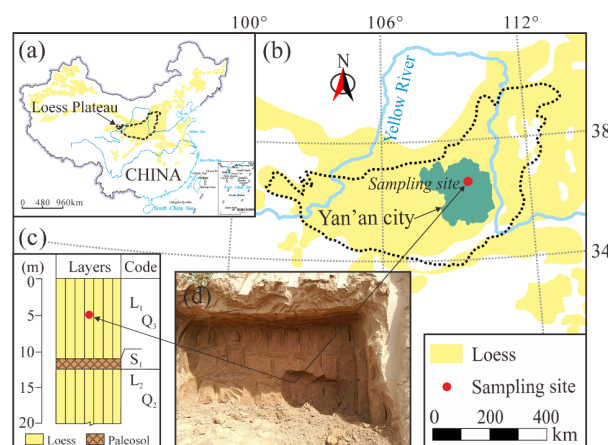


Fig. 1 Location map: (a) distribution of Loess Plateau in China; (b) sampling site in Yan'an, Loess Plateau of China; (c) soil profile at the sampling site (L represents loess and S represents paleosol); (d) a photograph of Q_3 loess at the sampling site.

and weakly cemented light-yellow windblown dust sediment that was deposited in the late Pleistocene (Li et al. 2018). The natural Q₃ loess sample was cut into cylinders with a diameter of 15 cm and a height of 22.5 cm and then placed inside an iron bucket and sealed with plastic film to avoid disturbance and reduce water loss. The sample buckets were packed in sawdust-filled boxes and transported to the laboratory to perform the various tests. The physical and mineralogical characterization of the tested loess is listed in Table 1. The natural water content of the soil was 10.6%. From the dry density (1.31g/cm³) and specific gravity (2.70), the saturated water content was calculated to be 39%. A laser particle size analyzer (Mastersizer 2000, UK) was used to determine the soil particle size distribution, which showed that the sand, silt and clay fractions accounted for 3.5%, 83.9%, and 12.6%, respectively. XRD was performed to determine the mineralogical composition of the loess sample using a D/max-2500 (Japan, Rigaku Corporation) X-ray diffractometer. After passing through a No. 200 sieve, the dried powder sample was scanned continuously between θ values of 5° and 56° with a step size of 0.02° under excitation energies of 40 kV and 200 mA. Jade software was used for qualitative and semiquantitative data analysis in terms of the Powder Diffraction File (PDF) database and adiabatic method. The XRD results showed that the tested sample is mainly composed of quartz, feldspar and calcite, with small amounts of amphibole,

dolomite, illite, chlorite and pyrite. Carbonate minerals and clay minerals account for 18.4% and 13.5%, respectively, and their hydrophilicity has a great influence on the physical and mechanical properties of the loess.

2.2 Tests procedures

Comprehensive experiments, including oedometer tests, SEM tests and MIP tests, were conducted on loess samples collected from the Yan'an area to study their multiscale characteristics of wetting deformation. Oedometer tests were performed to investigate the macroscopic characteristics of wetting deformation, SEM tests were performed to interpret the microstructure morphology, and MIP tests were performed to determine the pore structure characteristics.

2.2.1 Oedometer tests

A series of GDG-4S triplex high-pressure consolidometer instruments were used to perform double oedometer tests on natural loess to investigate the influence of the water content and vertical pressure on its compression, collapsibility and wetting collapse characteristics. The natural samples were cut by steel rings with a height of 20 mm and a diameter of 79.8 mm following the direction marked at the sampling site. Oedometer samples with initial water contents (w_o) of 6, 10 (natural), 14, 18, 26, 30, 34 and 39% (saturated) were prepared by air drying (for $w_o = 6\%$) and spraying. After spraying a predetermined amount of distilled water on the samples with filter paper and permeable stone placed at the top and bottom, the samples were wrapped with several layers of plastic film and placed in a humidifier for more than 48 h to achieve moisture homogenization. Among these samples, a saturated sample was achieved by fully inundating the sample prepared in advance to the liquid limit water content in the consolidometer cell. All 8 samples were progressively loaded up to increasing vertical pressures of 12.5, 25, 50, 100, 200, 300, 400, 600, 800, 1000, and 1200 kPa. The compression deformation under each vertical pressure was considered stable until it was less than 0.01 mm/h. To acquire more accurate results, one parallel control test with the same stress path was conducted, and the average values of parallel test results were taken as the baseline for subsequent analysis. Referring to the

Table 1 Physical and mineralogical characterization of the tested loess.

| Property | Value |
|--------------------------------------|-------|
| Specific gravity | 2.70 |
| Natural density (g/cm ³) | 1.45 |
| Natural water content (%) | 10.6 |
| Atterberg limits | |
| Liquid limit (%) | 29.78 |
| Plastic limit (%) | 17.96 |
| Plasticity index (%) | 11.82 |
| Particle size distribution (%) | |
| Sand > 0.075 mm | 3.5 |
| Silt 0.075–0.005 mm | 83.9 |
| Clay < 0.005 mm | 12.6 |
| Main minerals (%) | |
| Quartz | 47.3 |
| Feldspar | 19.0 |
| Amphibole | 1.1 |
| Calcite | 15.8 |
| Dolomite | 2.6 |
| Illite | 6.5 |
| Chlorite | 7.0 |
| Pyrite | 0.7 |

definition of the collapsibility coefficient δ_s , the wetting deformation coefficient δ_s' can be calculated from the difference in compression deformation between the initial water content w_o and the wetting water content w under the same vertical pressure p , as shown in Eq. 1. The traditional collapsibility coefficient is the wetting deformation coefficient of the sample when it is wetted to saturation.

$$\delta_s' = \frac{h_p - h_p'}{h_o} \quad (1)$$

where h_p and h_p' are the stabilized heights of the loess samples with the initial water content w_o and wetting water content w under the same p , respectively, and h_o is the initial height of the sample (20 mm in this study).

Finally, oedometer tests were conducted on the loess samples with an initial (natural) water content of 10% under nonwetting and saturated conditions at vertical pressures of 100, 200, 400 and 800 kPa. Considering the strain applied via the continuous loading curve mentioned above, it is important to select the data whose strain difference is less than $\pm 1\%$ under the same pressure; otherwise, the samples should be retested. The samples that produced valid data were sealed and stored in a humidifier to avoid disturbance before performing the microstructure tests.

2.2.2 SEM tests

A Phenom ProX scanning electron microscope (Netherlands, FEI Company) was used to directly characterize the surface microstructure of the natural water content samples in the initial state and under nonwetting and saturated conditions after the oedometer tests at vertical pressures of 100, 200, 400 and 800 kPa. The central parts of these samples were carefully cut into cubes with a volume of 2 cm³ (1 cm × 1 cm × 2 cm) using a thin-walled blade. Before microstructural observation, these subsamples were dehydrated in an Alpha1-2/LD-Plus freeze dryer (Germany, Marin Christ) using liquid nitrogen at a temperature below -50°C to minimize the influence of volume shrinkage due to water loss on the soil structure (Romero and Simms 2008; Jiang et al. 2014b; Shao et al. 2018). Afterward, the freeze-dried subsamples to be scanned were broken off to expose a fresh fracture plane, blown clean with a bulb syringe and then sprayed with gold, and several relatively flat areas on the fracture plane were selected to record the SEM images. Representative SEM observations of the

vertical plane of the samples were chosen for microstructural morphology interpretation.

2.2.3 MIP tests

An Auto Pore IV 9500 porosimetry apparatus (USA, Micromeritics Instrument Corporation) was used to measure the pore size distributions of the natural water content samples in the initial state and under nonwetting and saturated conditions after the oedometer tests at vertical pressures of 100, 200, 400 and 800 kPa. The samples to be tested were cut into cubes with a volume of 1 cm³, and the soil cubes were dehydrated following the procedure used for the SEM tests.

The principle of the MIP method for measuring the pore size distribution in soils is that the noninfiltrating liquid (i.e., mercury) will not flow into the soil pores without external pressure. Based on a simplified assumption of cylindrical pores, the pressure P_{Hg} required to intrude mercury into pores with radius r satisfies the Washburn equation (Washburn 1921), as shown in Eq. 2.

$$P_{Hg} = \frac{-2\gamma\cos\theta}{r} \quad (2)$$

where γ is the surface tension of the mercury and θ is the contact angle between the mercury and soil particles. In this study, $\gamma = 0.485$ N/m and $\theta = 130^\circ$ (Monroy et al. 2010; Jiang et al. 2014b; Wang et al. 2020a; Li et al. 2020). This means that when γ and θ remain unchanged, the lower the pressure is, the larger the pore diameter into which mercury can intrude. The mercury pressure in this study was raised in steps from 0.44 to 60,000 psia (approximately, 3.03 kPa-414 MPa) in terms of a low-pressure unit (0.44-30 psia) and a high-pressure unit (30-60,000 psia), corresponding to a pore diameters of 411-0.003 μm .

3 Results and Analyses

3.1 Macroscopic characteristics of wetting deformation

3.1.1 Compression

Fig. 2 shows the compression curves of loess samples with different initial water contents. The void ratio e decreases with increasing initial water content w_o and vertical pressure p . Similar to the compression curve of overconsolidated soil, the compression curve

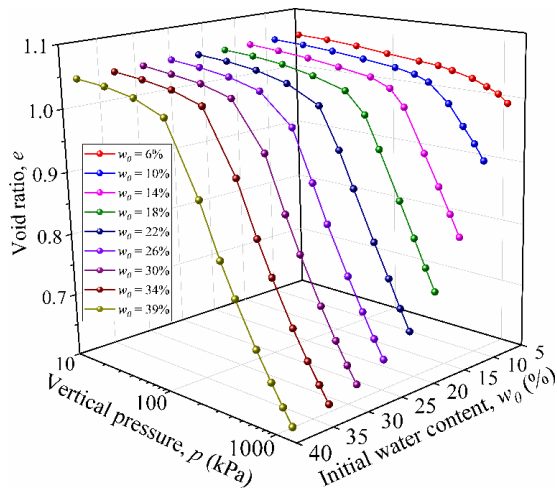


Fig. 2 Compression curves of loess with different initial water contents.

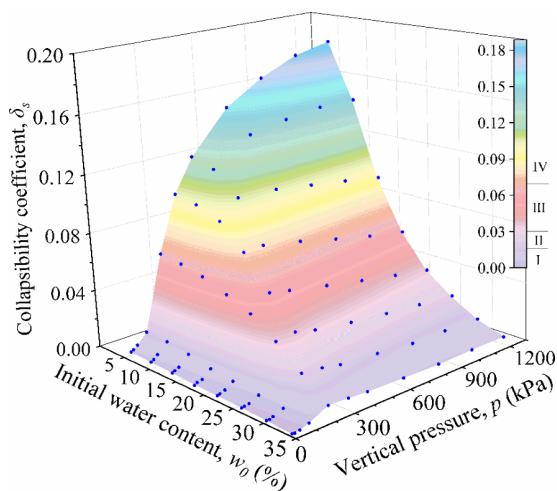


Fig. 3 Collapse surface of loess under different initial water contents and vertical pressures.

I, noncollapsibility ($\delta_s < 0.015$); II, weak collapsibility ($0.015 \leq \delta_s \leq 0.03$); III, moderate collapsibility ($0.03 < \delta_s \leq 0.07$); IV, strong collapsibility ($\delta_s > 0.07$).

of loess has an obvious inflection point, which divides the e - lgp curve into two segments: gentle and steep descent segments. In the gentle segment, the change in e under continuous loading is relatively small, which shows the characteristics of low plasticity. In the steep descent segment, e decreases more significantly with an increase in p , which indicates that the compression of soil clearly occurs and its plasticity increases under loading. Natural intact loess deposited in arid or semiarid conditions is an undercompacted soil with structural strength. Its unique microstructural characteristics support the loess to maintain the existing structural state without collapsing or slipping under the action of self-weight.

This effect is characterized by the "discontinuation" of the consolidation process, i.e., the gentle segment corresponding to a small deformation on the e - lgp curve. The stress that enables the "continuation" of the consolidation of loess is known as yield stress of structured soil (Chen et al. 2006; Jiang et al. 2012). After exceeding this stress, the soil structure begins to break down, and the deformation increases, which is illustrated by the steep descent segment corresponding to a large deformation on the e - lgp curve. Fig. 2 also shows that with increasing w_0 , the stress corresponding to the turning point on the e - lgp curve (i.e., yield stress of structured soil) decreases. This result shows that the compression of loess is water sensitive; which is characterized by a high strength and small deformation when w_0 is low. Wetting can accelerate the structural damage that occurs in loess as a response to loading, resulting in a reduction in strength and increase in deformation, which is closely related to the weakening of inter-particle cementation (Yang 1989; Ng et al. 2017; Li et al. 2019a; Mu et al. 2020) and capillary effects on the water-air interface (Mu et al. 2018; Gu et al. 2019). The structural stability of natural loess is related to not only its initial water content but also its dry density and clay content (Wei et al. 2019; Wang et al. 2020a).

3.1.2 Collapsibility

Fig. 3 shows the collapse surfaces of loess under different initial water contents (w_0) and vertical pressures (p) based on the test data. With increasing w_0 and p , the loess in the study area exhibits noncollapsibility (i.e., I: $\delta_s < 0.015$), weak collapsibility (i.e., II: $0.015 \leq \delta_s \leq 0.03$), moderate collapsibility (i.e., III: $0.03 < \delta_s \leq 0.07$) and strong collapsibility (i.e., IV: $\delta_s > 0.07$), according to China National Standards GB50025-2018 (Standardization Administration of China, Ministry of Housing and Urban-Rural Construction, 2018). The initial water content and vertical pressure impact the loess collapsibility. Generally, the smaller the initial water content is, the stronger the collapsibility, and the higher the sensitivity of the collapsibility coefficient to the pressure. However, at higher pressures, stronger collapsibility is not guaranteed. When w_0 is low ($w_0 < 14\%$), δ_s increases gradually with p , but its rate of increase slows; however, when w_0 is high ($w_0 > 14\%$), δ_s increases first and then decreases with increasing p . Moreover, the rate of the increase in δ_s

in the low-pressure section is faster than that of the decrease in δ_s in the high-pressure section; additionally, and the curve clustering in the low-pressure section is denser than that in the high-pressure section, which suggests that δ_s in this section is more sensitive to p and less sensitive to w_o (i.e., wetting). Fig. 3 shows that with an increase in w_o , the inflection point intensities or peak point intensities of the collapsibility coefficient curve decrease and shift to the left, indicating that the peak collapsibility pressure and peak collapsibility coefficient decrease with increasing w_o . The peak collapsibility pressure and peak collapsibility coefficient are mechanical parameters that reflect the loess structural characteristics during the wetting collapse process. These parameters represent the inter-particle cementation strength (including capillary force) and the maximum collapsibility of loess at a certain water content, respectively. The peak collapsibility pressure decreases with increasing w_o in the soil, is positively correlated with the yield stress under corresponding conditions and is slightly larger than the yield stress of the soil. This finding shows that after the soil structure yields, wetting can still cause collapse deformation, which also includes the slippage of some particles. This phenomenon suggests that some shear deformation occurs during loess collapse (Yang 1989; Jiang et al. 2014a), in addition to the compression deformation caused by pore compaction. Lin (1995) holds that the initial collapse pressure p_{sh} is the residual structural strength of soil (i.e., the water-stable cementation strength between particles). Fig. 3 shows that when the applied vertical pressure is lower than the yield stress of the saturated loess, the soil does not collapse under wetting conditions. At this time, the generalized p_{sh} can be understood as the

yield stress of saturated natural loess. If the yield stress of saturated loess is high, then it is difficult for the soil to collapse. When the external load exceeds the yield stress of saturated loess, the loess will undergo collapse, and the higher the vertical pressure and the smaller the initial water content are, the larger the loess collapsibility range. In summary, the initial collapse pressure of natural loess at any initial water content is close to the yield stress of the soil in its saturated state, while the peak collapse pressure is positively correlated with its own structural yield stress. Similar results were also observed from oedometer tests in previous studies conducted by Jiang et al. (2012) and Ma (2017).

3.1.3 Wetting collapse

Fig. 4 shows the representative relationship between the wetting deformation coefficient δ'_s and the wetting water content w of the loess sample under different vertical pressures (p). With an increase in w , δ'_s shows two stages: gentle period and growth period. The lower the pressure p , the longer the gentle period is, and the shorter the growth period is. With an increase in p , the gentle period becomes shorter or disappears, the growth period becomes longer, and its growth rate increases. When the soil is wetted to saturation, δ'_s reaches the maximum value (i.e., δ_s). Fig. 4 shows that δ'_s decreases with increasing initial water content w_o . When w_o is small, δ'_s increases with an increase in p , and the wetting sensitivity is weak at a low stress level but strong at a high stress level. In other words, the "microwetting effect" is significant at high pressures and a small amount of wetting can cause the collapse and large deformation of loess samples. This finding is in agreement with those of previous studies conducted by Chen et al. (2006) and

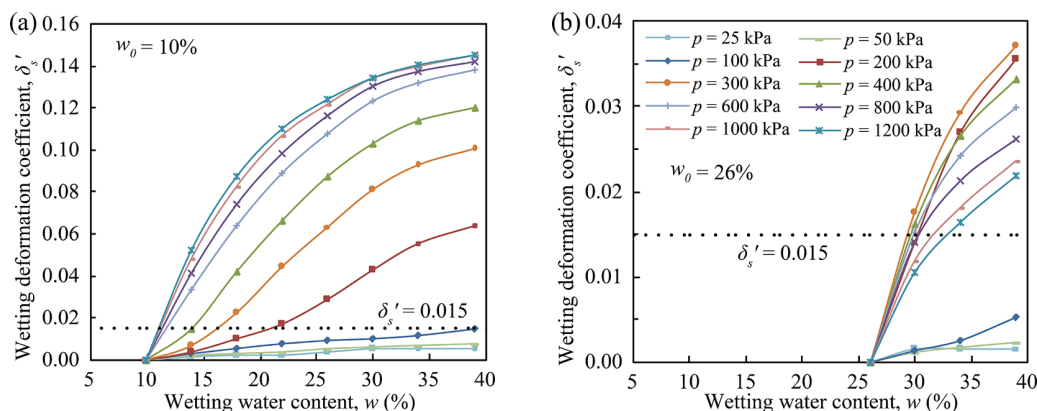


Fig. 4 Relationship between wetting deformation coefficient δ'_s and wetting water content w . w_o , initial water content; p , vertical pressure. $\delta'_s = 0.015$ is the critical line of loess wetting collapse.

Yang et al. (2017). When w_o is large, δ_s' increases with increasing p in the low pressure range but remains unchanged or decreases with increasing p in the high pressure range. In other words, with an increase in w_o , the initial point of the wetting sensitivity shifts from high pressure to low pressure, and the influence of p on δ_s' is gradually weakened. The minimum wetting water content, which is required when δ_s' of the loess samples with different water contents reaches 0.015 under a certain stress, is called the initial collapse water content w_{sh}' . Fig. 4 indicates that when w_o is small, w_{sh}' decreases monotonically with increasing p . When w_o is large, w_{sh}' decreases first and then increases with increasing p . The wetting level ($w_{sh}' - w_o$) required for the soil sample to collapse under a certain stress first decreases and then increases with an increase in w_o , and the higher the pressure is, the smaller the reduction range of $w_{sh}' - w_o$.

Fig. 5 shows the representative relationship between the wetting deformation coefficient δ_s' and the vertical pressure p of the loess sample under different wetting water contents (w). The relationship between δ_s' and p presents two different trends: (1) When w_o is small, δ_s' increases gradually with an increase in p , but its rate of increase slows. (2) When w_o is large, with an increase in p , δ_s' initially increases and then gradually decreases. The difference between these two responses is related to mainly the yield stress of the structured soil at different initial water contents. When the initial water content of the sample is large (Fig. 5b), the yield stress decreases (Fig. 2). At this time, when the applied vertical pressure is greater than the yield stress, the soil structure yields and the compressive strain increases rapidly, resulting in a decrease in strain induced by wetting (a decrease in the difference between the strains before and after wetting). Therefore, δ_s' decreases with increasing p after reaching a peak near the yield stress of the soil sample, thereby leading to the termination wetting collapse pressure (the maximum pressure required when $\delta_s' = 0.015$). Referring to the definition of the initial collapse pressure p_{sh} , the minimum pressure required when δ_s' reaches 0.015 is called the initial wetting collapse pressure p_{sh}' . Fig. 5 shows that with an increase in w , p_{sh}' decreases gradually, and the termination wetting collapse pressure increases gradually, indicating that the pressure range within which wetting collapse can occur in loess soil increases gradually. According to the calculation results of Fig. 5, the relationship between the initial

wetting collapse pressure p_{sh}' and the wetting water content w of loess samples with different initial water contents w_o can be obtained, as shown in Fig. 6. p_{sh}' decreases in the form of a power function with increasing w . When w is greater than 18% (i.e., plastic limit water content), the rate of decrease in p_{sh}' slows. When the soil is wetted to saturation, p_{sh}' is

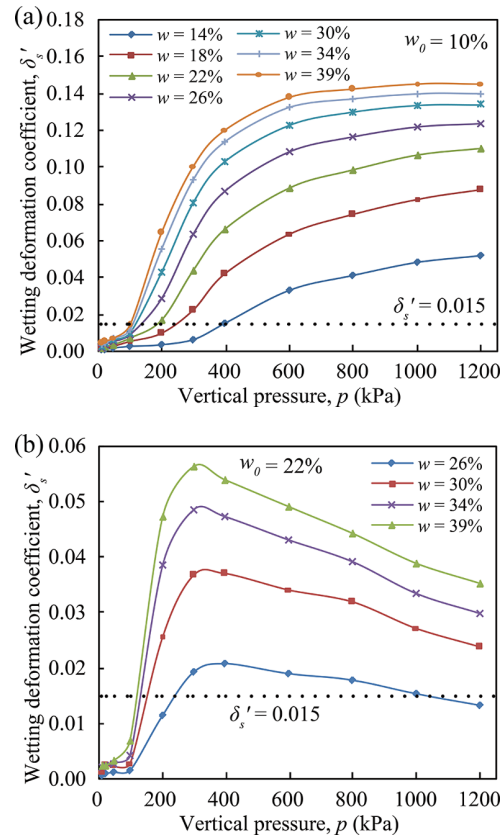


Fig. 5 Relationship between wetting deformation coefficient δ_s' and vertical pressure p . w_o , initial water content; w , wetting water content. $\delta_s' = 0.015$ is the critical line of loess wetting collapse.

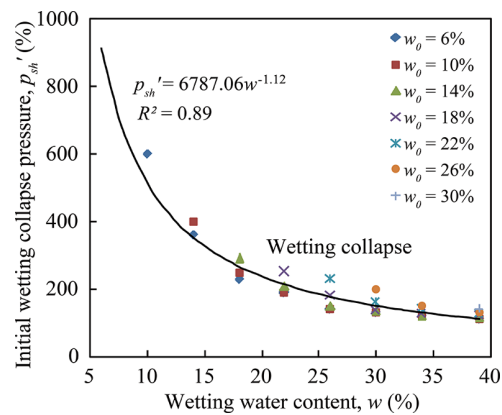


Fig. 6 Relationship between initial wetting collapse pressure p_{sh}' and wetting water content w . w_o , initial water content.

minimized, and is equivalent to p_{sh} . For a certain natural loess, the change in w_o has little effect on p_{sh} , which is the yield stress of structured soil under the saturated condition mentioned above. According to Fig. 6, the wetting deformation zone of loess can be divided into two parts, and whether loess with a certain initial water content will undergo wetting collapse can be judged by the stress level and the wetting water content.

3.2 SEM observations of loess samples before and after oedometer tests

Fig. 7 shows 1000× SEM images of natural loess in the initial state. The sands, silts and clays are combined to constitute the skeleton grain structure of the loess. Coarse particles with different shapes (such as angular, subangular, subrounded and flaky) can be clearly identified. The edges and surfaces of some silts are rather clean, while some silts are coated and wrapped with clay particles (or small-sized clay aggregates) or secondary carbonates. In addition, some aggregates (silt-clay aggregates and clay aggregates) developed under the action of cementations, matric suction and molecular attractions (Wang et al. 2020a) are distributed in the tested loess. These coarse particles and aggregates are arranged randomly and are connected via direct point contact or bridges composed of clay particles and clay aggregates. These features lead to loose and porous loess. According to the different particle patterns and their contact relations, the original pores in loess can be divided into intra-aggregate pores, mosaic pores formed by an intersecting arrangement of particles, and overhead pores formed by an arch-shaped arrangement of particles (Gao and Gao 1980; Lei 1988). The abundant overhead pores among aggregates or clean coarse particles are well developed, exhibiting good connectivity and high particle mobility. Thus, an open, metastable and non-water-stable overhead structure system of natural loess is formed.

Fig. 8 shows 1000× SEM images of the loess samples under nonwetting and saturated conditions consolidated under different vertical pressures (p). On the whole, various types of pores can still be observed in the samples under nonwetting conditions after consolidation (Figs. 8a, b, c and d). With an increase in p (Fig. 8d), the overhead pores in soil will not be completely compressed or disappear, but the

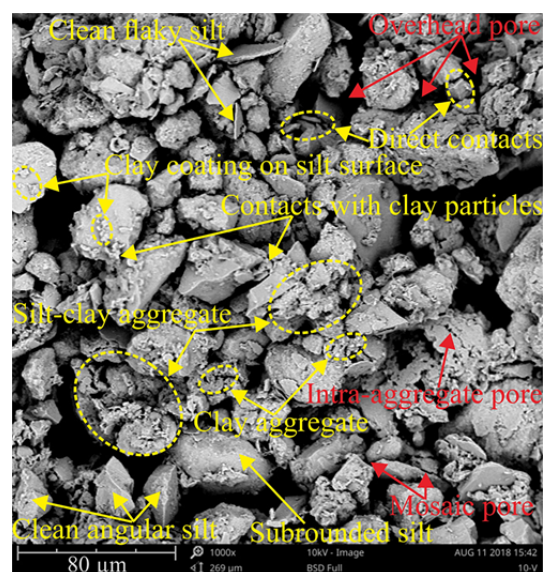


Fig. 7 Scanning electron microscopy images (1000×) of natural loess in the initial state.

number of particles that form the overhead pores under high-pressure conditions decreases, and the contact area between these particles increases. The total pore volume in the soil is compressed under loading. Direct point contact and partially weakly cemented particle connections are destroyed due to loading, resulting in the dislocation, rotation and rearrangement of particles. Because the initial moisture content in the soil is low, not wet, the cementing materials at the contacts and on the surfaces of the particles do not increase significantly, especially under low stress conditions (remain almost unchanged). Figs. 8e, f, g and h shows the microstructure of loess samples under saturated conditions after consolidation varying degrees. When p is 100 kPa (Fig. 8e), because the sample has not fully collapsed after inundation, the well-connected pores are still visible, and the surfaces of the particles are coated with a small amount of clays. With an increase in p , the boundary of skeleton particles in the samples is more blurred and broken, and the amount of small debris and clays increases at the contacts and on the surfaces of the particles. Particles are bonded tightly by these cementing materials, and the face contact between particles is obvious. Meanwhile, the overhead pores decrease notably, and smaller and fragmented pores are dominant in the samples. The clays and debris in the pores increase, the connectivity of the pores decreases and the pores become narrow. Correspondingly, the initial open and loose overhead structure of the soil nearly disappears,

forming a more uniform and closer structure with mosaic cementation. With increasing p , this microstructural change becomes more significant. This observation is consistent with the results of loess collapsibility determined using double oedometer tests.

3.3 Changes in pore characteristics from MIP

3.3.1 Pore classification of natural loess in the initial state

Fig. 9a shows the cumulative pore volume of a loess sample in the initial state in a semilogarithmic plot. In fact, in a statistical sense, soil pore structures have fractal features including self-similarity (Mandelbrot 1982). Therefore, fractal geometry theory, which is independent of scale, can be used to

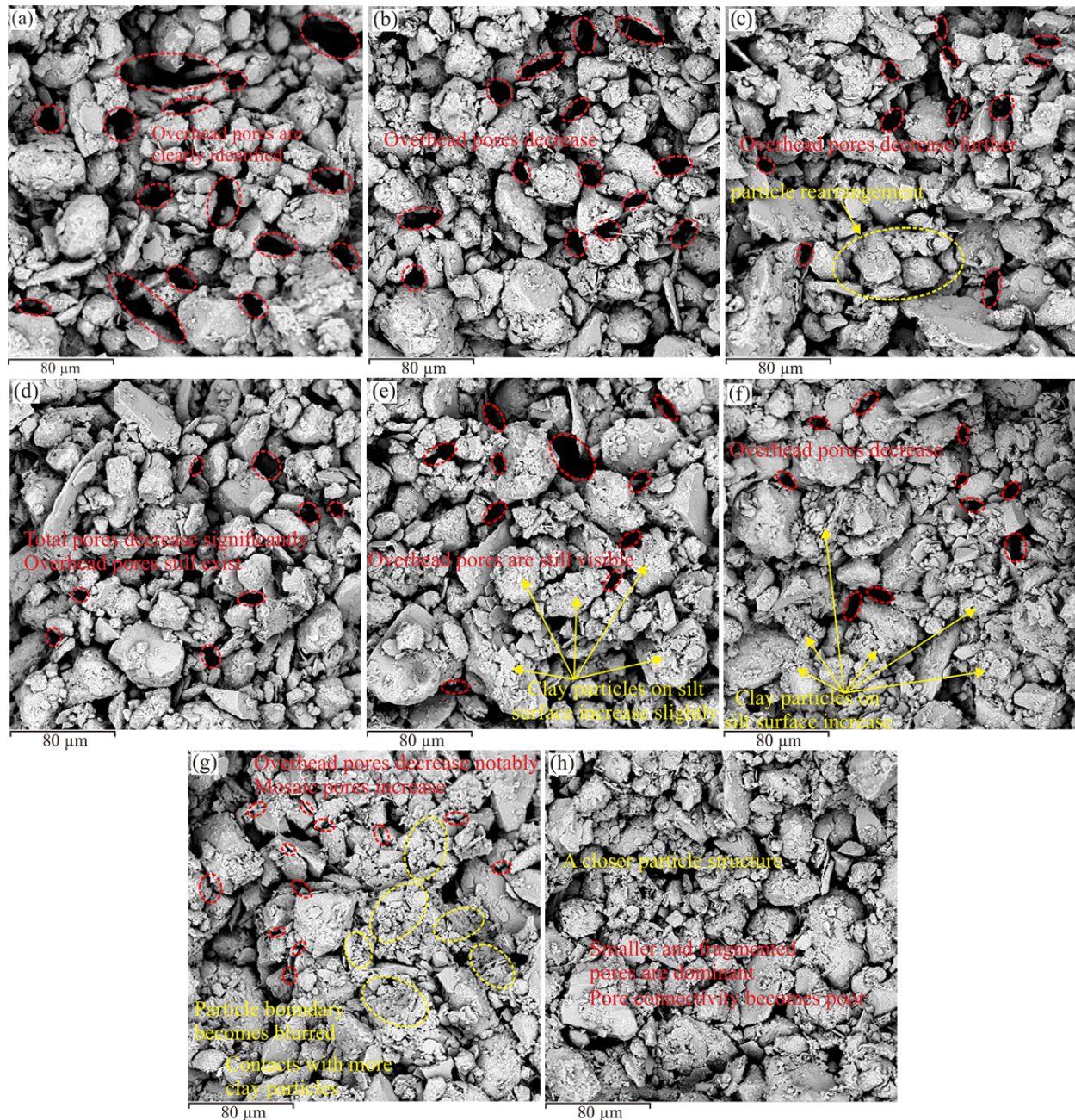


Fig. 8 Scanning electron microscopy images (1000 \times) of samples under nonwetting and saturated conditions consolidated at different vertical pressures (p): (a) $w_o = 10\%$, $p = 100$ kPa; (b) $w_o = 10\%$, $p = 200$ kPa; (c) $w_o = 10\%$, $p = 400$ kPa; (d) $w_o = 10\%$, $p = 800$ kPa; (e) $w_o = 39\%$, $p = 100$ kPa; (f) $w_o = 39\%$, $p = 200$ kPa; (g) $w_o = 39\%$, $p = 400$ kPa; (h) $w_o = 39\%$, $p = 800$ kPa. w_o , initial water content.

quantitatively describe the complex distribution characteristics of loess pores, to essentially reveal the mechanical behavior and failure mechanism of soil (Wang and Wang 2000). Referring to the volume fractal model (Wang and Wang 2000; Ma 2017), the double logarithm relationship between the percentage of cumulative pore volume with diameter less than D (i.e., V_D) in total pore volume (i.e., V) and pore diameter D , i.e., $\log(V_D / V) - \log D$, is shown in Fig. 9b.

In Fig. 9b, the curve does not have a uniform slope but a characteristic of linear stages. The curve is divided into four parts by three different inflection points, namely, 0.05, 2.5 and 14 μm , and each part has a fixed slope, which indicates that the pore size distribution of loess has multifractal characteristics and that the pores represented by each part of the curve are self-similar. Therefore, the three boundary points can be used as characteristic pore sizes to distinguish the similar pores in each interval. The pores of the corresponding intervals are called micropores, small pores, mesopores and macropores in terms of the relative pore sizes. This provides a scientific basis for the pore classification of the tested loess. These four types of pores in loess have their own structural characteristics and formation mechanisms. As shown in the SEM images (Fig. 7), the micropores correspond to intra-aggregate pores, small pores correspond to mosaic pores, mesopores correspond to overhead pores, and macropores correspond to large overhead pores and secondary pores (residual mineral leaching pores, root holes, wormholes, rat holes, fissures and joints, Lei 1988). According to the results of the MIP tests and the classification method, the proportion of mesopores

(2.5-14 μm) in the intact loess reaches 62.62%, followed by 17.24% small pores (0.05-2.5 μm), 10.37% micropores (< 0.05 μm) and 9.77% macropore pores (> 14 μm).

3.3.2 Changes in pore size distributions and characteristic pore diameters

Fig. 10 provides the pore size distributions in terms of the pore size density functions for loess samples before and after oedometer tests under different vertical pressures (p). The pore size density function is derived from the derivative of the cumulative pore volume V with respect to the logarithm of the pore diameter D , i.e., $dV/d\log D$, mL/g. Fig. 10 shows that the pore size distributions of all the samples exhibit a bimodal structure represented by the intra-aggregate pore and inter-aggregate pore populations, except for the local anomalous minimum points in the low-to-high pressure transition zone. These two local peaks divide the whole pore interval into several sections, and each section represents a corresponding pore structure and formation mechanism. The small pore size corresponds to the relatively low peak, and the peak band curves almost coincide (the peak intensities of the samples before and after wetting to saturation decrease slightly compared with that of the initial state). The dominant pore diameter at the low peak is approximately 0.03 μm , i.e., the intra-aggregate pore sizes and the corresponding peak intensities remain basically unchanged during the process of wetting collapse under loading. The large pore size corresponds to the steep peak, which changes slightly before wetting but changes greatly after wetting to saturation. The peak point shifts uniformly from

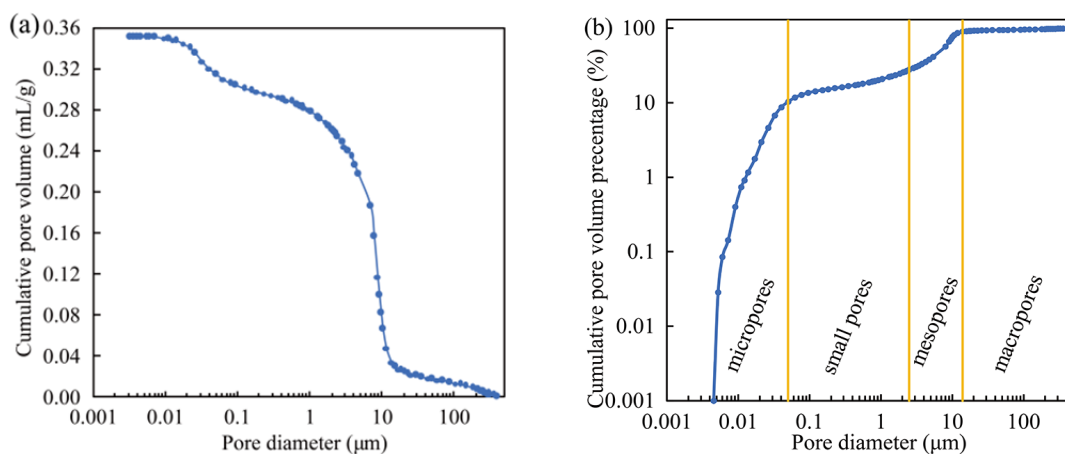


Fig. 9 Cumulative pore volume curve of a sample in the initial state: (a) in a semilogarithmic plot; (b) in a double logarithmic plot.

approximately 9 μm of the initial sample to the direction of pore diameter reduction. Additionally, with increasing p , the shift increases, the peak intensity decreases, and the gentle curve between these two peaks rises gradually, i.e., the inter-aggregate pore populations decrease and transform each other, and the reduction increases with increasing p (stronger collapse). When p is 100 kPa, the loess is not fully collapsible, so the pore size distribution changes little after wetting to saturation. These findings are in agreement with the SEM results in Fig. 8. Fig. 10 shows that with loading, the collapsibility of loess is mainly reflected in the effect

of wetting on the pore size distribution characteristics (inter-aggregate pore populations), while the pore size distribution of the soil with a low w_o before wetting changes little.

Table 2 presents the characteristic pore diameters before and after oedometer tests under different vertical pressures (p) and their relationship with saturated collapsibility coefficient (δ_s). The threshold pore diameter is the pore size that corresponds to the first slope mutation point along the cumulative pore volume curve from right to left (Fig. 9a), which reflects the response of the larger pores to changes in the external environment. The

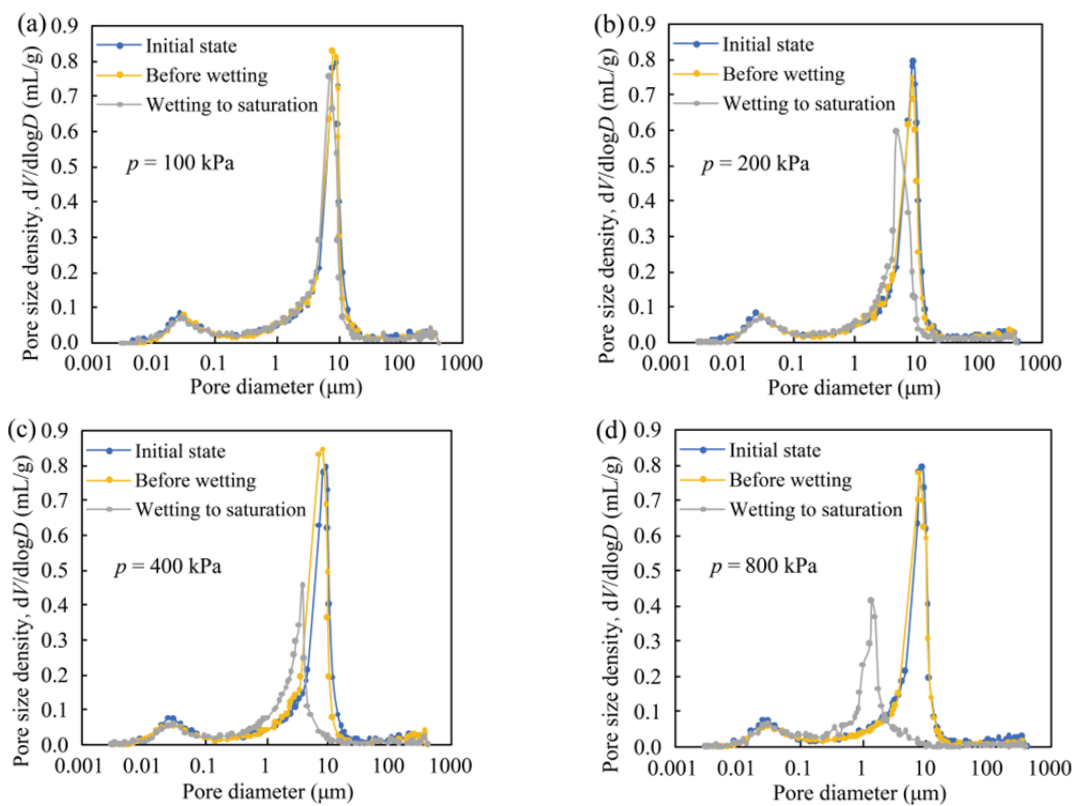


Fig. 10 Pore size distributions of samples before and after oedometer tests at vertical pressures (p) of 100 kPa (a), 200 kPa (b), 400 kPa (c) and 800 kPa (d). V , cumulative pore volume; D , pore diameter.

Table 2 Relationship between collapsibility coefficient (δ_s) and characteristic pore diameters under different vertical pressures (p).

| p (kPa) | δ_s | d (μm) | | | | | | | | | Δd (μm) | | |
|--------------|------------|-----------------------|----------|----------|-------|--------|-------|--------|-------|--------|------------------------------|--------------|--------------|
| | | d_{o1} | d_{o2} | d_{o3} | d_1 | d_1' | d_2 | d_2' | d_3 | d_3' | Δd_1 | Δd_2 | Δd_3 |
| 100 | 0.014 | 12.97 | 9.06 | 6.13 | 12.73 | 11.22 | 8.35 | 7.39 | 5.85 | 4.87 | 1.51 | 0.96 | 0.98 |
| 200 | 0.064 | | | | 12.62 | 8.66 | 8.16 | 4.88 | 5.42 | 3.46 | 3.96 | 3.28 | 1.96 |
| 400 | 0.120 | | | | 11.37 | 6.03 | 7.95 | 3.66 | 5.60 | 2.30 | 5.34 | 4.29 | 3.30 |
| 800 | 0.142 | | | | 12.83 | 4.97 | 8.03 | 1.45 | 5.76 | 1.02 | 7.86 | 6.58 | 4.74 |

Note: d_{o1} , d_1 , d_1' are the threshold pore diameters of samples in the initial state, before wetting and after wetting to saturation, respectively; d_{o2} , d_2 , d_2' are the most probable pore diameters of samples in the initial state, before wetting and after wetting to saturation, respectively; d_{o3} , d_3 , d_3' are the median pore diameters of samples in the initial state, before wetting and after wetting to saturation, respectively; and Δd_1 , Δd_2 , Δd_3 are the reductions in the characteristic pore diameters of samples during wetting to saturation.

most probable pore diameter is the pore size at the maximum volume (steep peak point) on the pore size distribution curve (Fig. 10), which represents the overall change in the pore size distribution. The median pore diameter is the corresponding pore size when the cumulative pore volume percentage reaches 50%, which reflects the dominant pore diameter in loess soils. With increasing p , the characteristic pore diameters of the sample before wetting (d_1 , d_2 and d_3) decrease slightly compared with those of the initial state (d_{01} , d_{02} and d_{03}), while the characteristic pore diameters of the sample after wetting to saturation (d_1' , d_2' and d_3') decrease greatly. Moreover, the larger the collapsibility coefficient is, the stronger the loess collapsibility, and the greater the reduction in the characteristic pore diameters before wetting and after wetting to saturation (Δd_1 , Δd_2 and Δd_3). As the pressure increases from 100 kPa to 200 kPa, the intact loess soil undergoes moderate collapse from noncollapse, and the characteristic pore diameters decrease most rapidly after the loess is wetted to saturation. As the vertical pressure increases, the rate of increase in δ_s decreases, and the rate of decrease in characteristic pore size during wetting to saturation also decreases (similar to the change in total pore volume). When the applied p reaches 800 kPa ($\delta_s = 0.142$), the threshold pore diameter, the most probable pore diameter and the median pore diameter decrease by 61.26% (from 12.83 μm to 4.97 μm), 81.94% (from 8.03 μm to 1.45 μm) and 82.29% (from 5.76 μm to 1.02 μm), respectively. Note that the reduction in the characteristic pore diameters due to wetting varies in the inter-aggregate pore populations with diameters larger than 0.05 μm .

3.3.3 Change in classified pore volume

Based on the above pore classification method, Fig. 11 presents the change in the classified pore volume of the samples during the oedometer tests under different vertical pressures (p). The volume of each type of pore in a samples before wetting (Fig. 11a) basically decreases under loading (small pores increase slightly by 0.0003 mL/g under $p = 200$ kPa). Among the pore volumes, the mesopore volume decreases the most, the small pore volume decreases the least, and the macropore volume decreases only slightly more than the micropore volume (which may be due to the same cementing materials and a similar strength between the particles that form the residual mineral leaching macropores and micropores). With

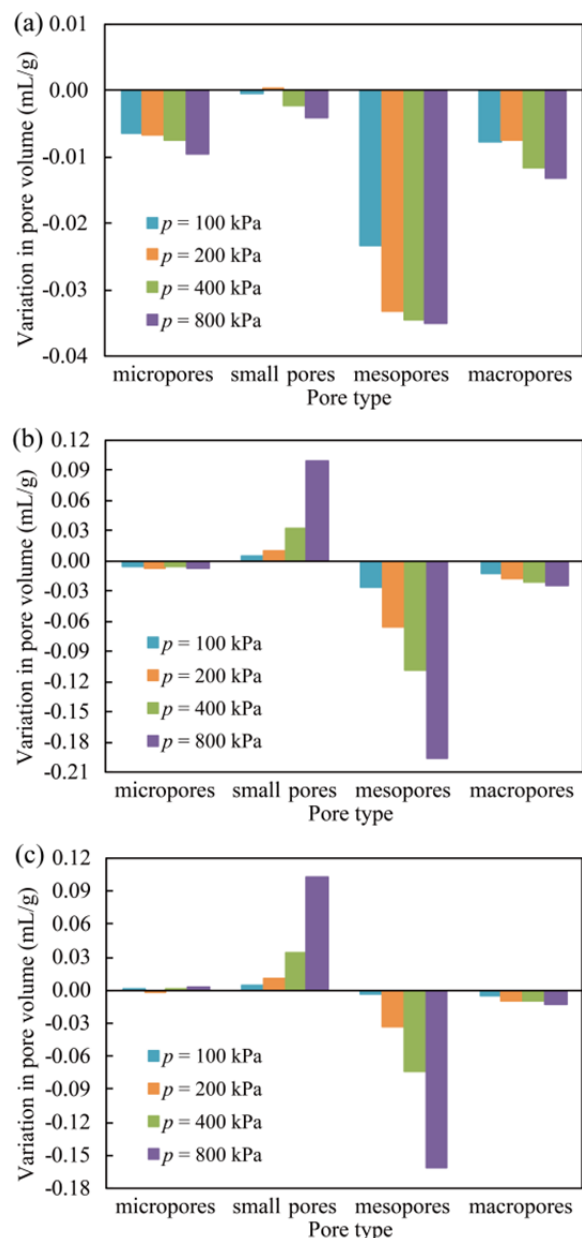


Fig. 11 Change in classified pore volume during oedometer tests under different vertical pressures (p): (a) samples before wetting; (b) saturated samples; (c) samples before and after wetting to saturation.

an increase in p , the reduction in volume of each type of pore increases gradually, which indicates that for samples before wetting, the load action is mainly reflected in the overall compression of its pores. With loading, the volume of the micro-, meso- and macropores of samples under saturated conditions (Fig. 11b) decreases, and the volume of the small pores increases. Among these pores, the volume of mesopores and small pores varies greatly. With

increasing p , the volume change in the small pores, mesopores and macropores increases further, while the volume of micropores decreases slightly (average of -0.006 mL/g). By calculating the total pore volume change in samples before wetting and after wetting to saturation before loading to their own yield stress, the total pore volume change in the sample before wetting is 0.0527 mL/g, and that of a sample under saturated conditions is 0.0498 mL/g. Although the change in the classified pore volume is different, the total pore volume change is basically the same, which indicates that the change in the soil pore structure is closely related to its structural yield response. Fig. 11c shows that the main types of pores with large volume changes during wetting to saturation are the small pores, mesopores and macropores, whereas the volume of micropores remains almost unchanged (increases slightly by 0.0012 mL/g on average). Among them, the volume of mesopores and macropores decreases, and the volume of small pores increases. With increasing p , the volume change in mesopores and small pores increases gradually, while the volume reduction in the macropores first increases and then remains basically unchanged

(approximately -0.01 mL/g), which can be attributed to the fact that some secondary macropores cemented by aged calcium carbonate have a certain stability and are not easily deformed (Lei 1988; Wang et al. 2020a). These findings further indicate that during the process of wetting collapse in soil, the intra-aggregate pores (i.e., micropores) remain basically unchanged, which is mainly due to the reduction and mutual transformation of the inter-aggregate pore populations (i.e., small pores, mesopores and macropores).

4 Discussion

4.1 Analysis of the whole process of wetting deformation

The whole process of wetting deformation of loess samples with different initial water contents under loading is characterized by the $e-p$ curve, as shown in Fig. 12. The critical wetting collapse curve (see the black line) is drawn from the critical void ratio that corresponds to the initial collapse water

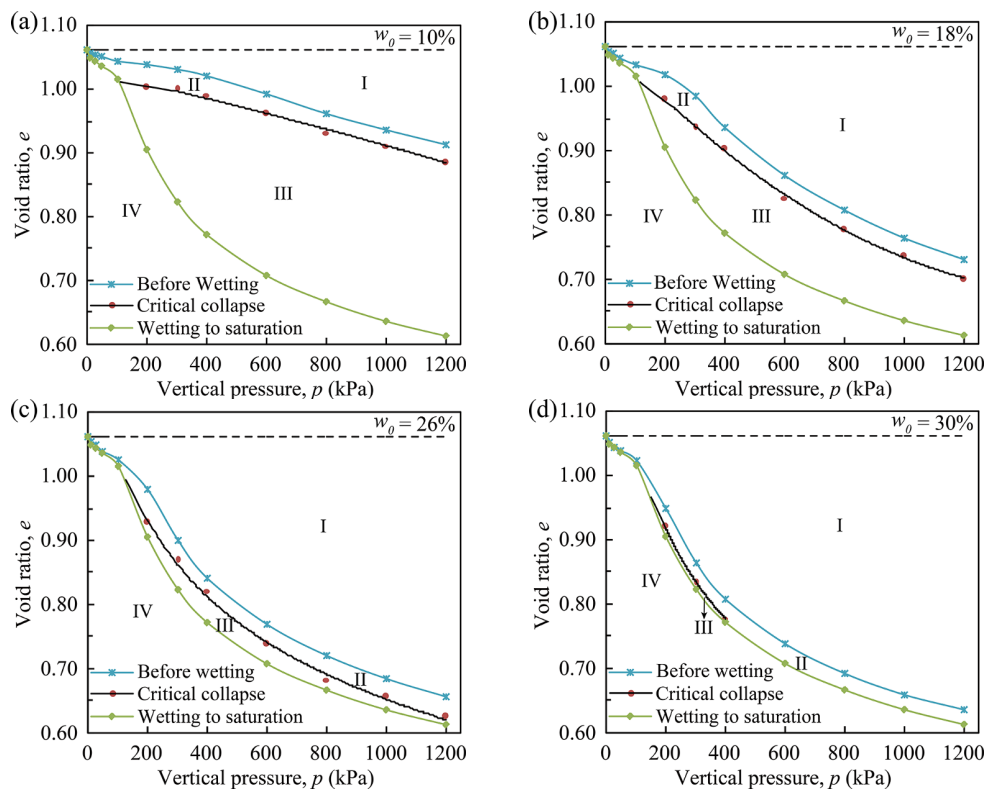


Fig. 12 Whole process of wetting deformation of samples with initial water contents (w_0) of 10% (a), 18% (b), 26% (c) and 30% (d) under loading. I, compression zone (i.e., nonwetting deformation zone); II, unsaturated wetting deformation zone; III, wetting collapse deformation zone; IV, no deformation zone.

content w_{sh}' (Fig. 4) under different vertical pressures. The other two curves are drawn from the void ratio of the samples before (see the blue line) and after wetting to saturation (see the green line) under different vertical pressures. These three curves divide the whole wetting deformation process of loess under loading into four zones: the compression zone (i.e., nonwetting deformation zone) (I), unsaturated wetting deformation zone (II), wetting collapse deformation zone (III) and no deformation zone (IV). Overall, as the initial water content increases, the range of I increases, the range of III decreases, the range of II decreases slightly, and the range of IV remains unchanged. When w_o is small, the range of II decreases slightly with an increase in p , while the range of III increases with an increase in p . When w_o is large, the range of II decreases initially and then increases with an increase in p , and the range of III first increases and then decreases with an increase in p . The range of I always increases with an increase in

p . In other words, the total deformation of intact loess with an initial water content of w_o after wetting to saturation can be predicted with certainty. With a change in w_o , the ranges of I, II and III change dynamically and transform each other with loading and wetting. For a given initial water content w_o , the loess does not necessarily need to be wetted to saturation for collapse to occur. Under different stresses, there exists a critical water content and critical void ratio that can cause collapse. When the wetting water content is greater than the critical water content or the void ratio is less than the critical pore ratio, the soil will collapse. In particular, more attention should be paid to the "microwetting effect" of loess with a small initial water content under high stress. Therefore, considering the different sensitivities to wetting under different stress levels, the development of wetting deformation can be predicted or controlled within the allowable limits of buildings or slopes to reduce or avoid collapse hazards by controlling the wetting level and rate (such as setting water-resisting layers with different permeabilities in the soil) (Yang et al. 2017), which is of practical significance for construction projects and hazard prevention in loess areas.

4.2 Microscopic mechanism of wetting deformation

Various loess engineering geology problems and the corresponding underlying mechanisms are often facilitated by changes in the compositional, microstructural and physicochemical properties associated with the mechanical behavior of loess under external environmental changes (Lei 1988; Liu et al. 2016; Li et al. 2018; Li et al. 2019b; Zhuang et al. 2020). The levels and elements of the loess microstructure, i.e., particles, cementation bonds, contact relations and pores, influence and restrict each other (Barden et al. 1973; Li et al. 2016), and jointly determine its mechanical behavior and engineering properties. The dynamic development process of the wetting deformation of loess reflects the different stages of soil microstructure damage and change (Chen et al. 2006) (Fig. 12). The change in microstructure of loess with a natural water content from the initial state to wetting collapse under loading is shown in Fig. 13. The natural unsaturated Malan loess has a unique open, metastable and non-water-stable overhead structure with high porosity, few

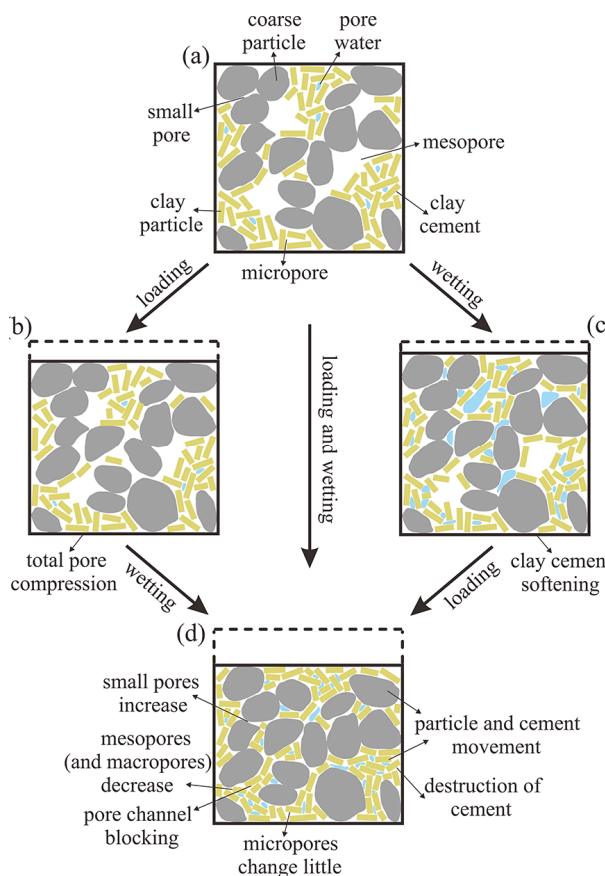


Fig. 13 Microscopic mechanism of wetting deformation: (a) microstructure system of natural loess in the initial state; (b) natural loess with loading; (c) natural loess with wetting; (d) wetting collapse under loading.

contacts, weak cementation and large particle mobility (Figs. 7 and 13a). Under a certain vertical stress, the pores in this soil are compressed overall (especially the abundant overhead pores), and the total pore volume decreases (Fig. 11a), while the dominant sizes of pores change only slightly (Fig. 10, Table 2), and there are still a certain number of overhead pores (Figs. 8a, b, c and d). At this time, the change in the cementing materials at the contacts and on the surfaces of the particles is not obvious (Fig. 13b). Subsequently, with loading, water immersion can accelerate the response and destruction of the particle connection to stress. When the water content in the soil increases (flows into the mesopores, which mainly affect suction changes, i.e., capillary water, see Muñoz-Castelblanco et al. 2011), on the one hand, the molecular attraction and capillary force (matric suction) of the shrink films on the water-air interface decrease (Mu et al. 2018; Gu et al. 2019); on the other hand, the hydrolabile cement (soluble salts and organic matter) in the loess almost dissipates, and clay aggregates or cements are scattered and destroyed due to thickening of the electric double layer on the clay surface, ion diffusion and expansion of the sample (Yang 1989; Li et al. 2019b; Mu et al. 2020). Additionally, carbonates and iron oxides are slowly leached and disintegrated under considerable water movement (Yang 1989; Xie et al. 2018). In turn, due to the loss of calcium carbonate, clay aggregates also become softer and disperse into small aggregates (Gao and Gao 1980). With the decrease in matric suction and the destruction of these interparticle cementations, other small proportions of hydrostabil cement become partially destroyed due to the stress concentrations induced under an external load (Yang 1989). Meanwhile, the scattered clays and debris move to the overhead pores and macropores under the external load or recombine and adhere to the particles due to the water movement (Figs. 8e, f, g and h). Then, the particles positions adjust, increasing the contact area and the resistance of the external load. As a result, the pore channels become blocked, the pore connectivity becomes poor, and the size and volume of pores in the soil decrease (decrease in meso- and macropores and increase in small pores) (Figs. 10 and 11c), resulting in a certain amount of deformation in the soil, i.e., volume contraction. When most of the interparticle cementation strength is lost due to an increase in the wetting level and pressure, the initial open metastable structure of loess

collapses completely (collapse chain reaction), and the soil undergoes macroscopic deformation (Xie et al. 2018); at the same time, a relatively stable and close structure is formed (Fig. 13d). In particular, under high-stress conditions, microwetting may cause a sharp decrease in the cementation strength between particles (Fig. 4), causing the overhead structure system of the soil to collapse rapidly. In this case, the loess soil instantaneously undergoes considerable deformation when the stress is constant. Throughout the process of the wetting collapse of loess under loading, water can weaken the interparticle cementation strength, decrease the soil suction, lubricate the soil particles and cause them to slide and deform continuously. However, when the collapsibility reaches a certain degree, the pore blocking and slow drainage of pore water (Yang 1989) in small pores with a better water holding capacity will reduce the collapse rate of loess. In addition, the sequence of loading and wetting (Jiang et al. 2012) only affects the degree of change in various microstructure levels and elements with different sensitivities, which has little influence on the final soil structure collapse (Figs. 13b, c and d).

Based on this investigation, the compression deformation is closely related to the loess loose overhead structure. The unique overhead structure system of loess is the precondition of collapse and provides space for it (Yang 1989). However, the wetting-induced deformation is more related to the degree of loss of the interparticle cementation strength. Therefore, the wetting collapse of loess soil is dependent on both microstructural and compositional characteristics (Liu et al. 2016; Xie et al. 2018; Li et al. 2019a; Wei et al. 2020). The wetting collapse of loess (including unsaturated wetting collapse) under loading depends on the changes in different microstructure levels and elements. This collapse chain reaction is manifested by cementation dissipation, scattering and recombination, particle deformation (slip, dislocation, crushing and peeling) and reorganization, pore channel blocking, inter-aggregate pore population reduction and mutual transformation, and macroscale volume contraction. This process is dependent on the initial water content, stress level and wetting degree. Based on these findings, in engineering practice, the collapsibility of loess can be reduced or eliminated by changing its loose overhead structure and cementation properties in certain ways (such as by applying acidic solutions,

salt solutions, dynamic compaction and prewetting loads), thereby reducing collapse settlement and preventing possible hazards (such as collapse cracks and pits and landslides).

Notably, different microstructure levels and elements respond differently to wetting collapse under loading. In terms of the pore levels, this study (Figs. 11 and 12, Table 2) shows that wetting-induced changes in intra-aggregate pores (i.e., micropores) are very small, which is mainly reflected in the decrease in the dominant size and volume of macropores and abundant mesopores and the increase in the volume of small pores (i.e., the reduction and mutual transformation of the inter-aggregate pore populations, Fig. 11c). This condition indicates that the macropores and mesopores in loess are active, unstable and prone to collapse upon loading and wetting, which causes the soil to produce corresponding macroscopic deformation. Conversely, the inert and stable intra-aggregate pores have little influence on the wetting collapse of loess. Shao et al. (2018) and Mu et al. (2020) also pointed out that the intra-aggregate pores in loess remain almost unchanged during wetting collapse. Therefore, further research on microstructural changes and mechanical responses of loess or other soils should first distinguish the microstructure levels and the elements of each level and then focus more on the microstructure layers and elements directly related to their macromechanical properties and potential mechanism, which may be more targeted and efficient.

Additionally, some researchers noted that MIP tests may underestimate the pore volume of soil (Wang et al. 2020a; Li et al. 2020; Mu et al. 2020). The limitations of the MIP tests in this study are mainly related to the following three aspects: (1) some pores are too large to be measured at the minimum pressure of the MIP device (i.e., undetected pores, > 411 μm); (2) some pores are too small for mercury to intrude into under the maximum pressure applied by MIP device (i.e., nonintruded pores, < 0.003 μm); and (3) fully enclosed pores cannot be measured. In general, the original pores (i.e., intra-aggregate pores, mosaic pores and overhead pores, refer to Gao and Gao 1980, Lei 1988, see Fig. 7) formed within the range of the loess particle size distribution are not larger than 411 μm . In addition, the nonintruded pores (< 3 nm) and enclosed pores have little influence on the mechanical behavior of loess since these pores are quite sparse, small and stable (Gao

and Gao 1980; Lei 1988). Therefore, although MIP tests are not able to measure all the pores in soil, the pore size distributions over the wide range of 0.003-411 μm (which mainly control the mechanical properties of loess) characterized by the MIP method used in this study are effective and reasonable for the study of loess wetting deformation characteristics. However, the above analysis is based on the assumption that pores are cylindrical, while SEM images show that the actual pore morphology in loess is complex. Thus, the findings in this study will be used as the basis for our future work focusing on the relationship between different pore morphologies and the mechanical behavior of natural loess.

5 Conclusion

Double oedometer tests were conducted on natural loess with various initial water contents (from natural to saturated) to investigate the effects of the water content and vertical pressure on the wetting deformation. SEM and MIP tests were conducted on samples with natural water contents before and after the oedometer tests to study the microstructural characteristics of wetting collapse. The main conclusions are as follows:

1. The compression and collapsibility of loess are affected by the initial water content and vertical pressure. Natural loess with a low initial water content exhibits a high strength and small deformation. Wetting can accelerate the structural damage and yield under loading, resulting in strength reduction accompanied by increasing deformation. The initial collapse pressure of natural loess at all initial water contents is close to the yield stress of the soil in its saturated state, while the peak collapse pressure is positively correlated with the yield stress of the soil itself.

2. The variations in the critical parameters for natural loess to wetting collapse were presented. The initial wetting collapse pressure of loess with different initial water contents decreases in the form of a power function with increasing wetting water content. The minimum wetting water content and the critical void ratio required for wetting collapse are related to the vertical pressure. Under higher vertical pressures, microwetting can cause a large deformation of loess with a small initial water content. Consequently, the whole wetting deformation process of loess under

loading is divided into compression (i.e., nonwetting deformation), unsaturated wetting deformation, wetting collapse deformation and no deformation.

3. The bimodal pore structure characterized by intra-aggregate pores and inter-aggregate pore populations is not eliminated with loading and wetting. The compression deformation is mainly attributed to the overall reduction in pore volume with increasing vertical pressure, while the dominant sizes of the pores change only slightly. Wetting conditions can result in a significant decrease in the dominant size and volume of macropores ($> 14 \mu\text{m}$) and abundant mesopores ($2.5\text{-}14 \mu\text{m}$) and an increase in the volume of small pores ($0.05\text{-}2.5 \mu\text{m}$) with increasing stress level and collapse potential, while the volume of micropores (i.e., intra-aggregate pores, $< 0.05 \mu\text{m}$) changes little. This condition indicates that the wetting collapse of loess under loading is greatly influenced by the active and unstable macropores and mesopores.

4. The wetting collapse of loess under loading depends on the changes in different microstructure levels and elements. This collapse chain reaction is manifested by cementation dissipation, scattering and recombination, particle deformation and

reorganization, pore channel blocking, inter-aggregate pore population (i.e., $> 0.05 \mu\text{m}$) reduction and mutual transformation, and macroscale volume contraction. This process is dependent on the initial water content, stress level and wetting degree.

The findings may provide insights into the wetting collapse and the underlying mechanisms of natural loess, thereby preventing loess collapse hazards and facilitating geological engineering construction. Moreover, the results considering the effects of pore structure on loess wetting collapse are the basis for our future work focusing on the relationship between other microstructure elements and the mechanical behavior of loess.

Acknowledgments

This research was supported by the Major Program of National Natural Science Foundation of China (No. 41790441), the National Natural Science Foundation of China (No. 41807234, 41907235), and the Fundamental Research Funds for the Central Universities, CHD (300102269203).

References

- Alfi AAS (1984) Mechanical and Electron Optical Properties of a Stabilized Collapsible Soil in Tucson, Arizona. PhD thesis, University of Arizona, Tucson, Arizona.
- Assallay AM, Rogers CDF, Smalley IJ (1997) Formation and collapse of meta-stable particle packings and open structures in loess deposits. *Eng Geol* 48(1): 101-115. [https://doi.org/10.1016/S0013-7952\(97\)81916-3](https://doi.org/10.1016/S0013-7952(97)81916-3)
- Barden L, McGown A, Collins K (1973) The collapse mechanism in partly saturated soil. *Eng Geol* 7: 49-60. [https://doi.org/10.1016/0013-7952\(73\)90006-9](https://doi.org/10.1016/0013-7952(73)90006-9)
- Chen CL, Gao P, Hu ZQ (2006) Moistening deformation characteristic of loess and its relation to structure. *Chin J Rock Mech Eng* 25(7): 1352-1360. (In Chinese) <https://doi.org/10.3321/j.issn:1000-6915.2006.07.009>
- Cheng Q, Zhou C, Ng CWW, et al. (2020) Effects of soil structure on thermal softening of yield stress. *Eng Geol* 269: 105544. <https://doi.org/10.1016/j.enggeo.2020.105544>
- Cui SH, Pei XJ, Wu HY, et al. (2018) Centrifuge model test of an irrigation-induced loess landslide in the Heifangtai loess platform, Northwest China. *J Mt Sci* 15(1): 130-143. <https://doi.org/10.1007/s11629-017-4490-0>
- Derbyshire E, Mellors TW (1988) Geological and geotechnical characteristic of some loess and loessic soil from China and Britain: a comparison. *Eng Geol* 25: 135-175. [https://doi.org/10.1016/0013-7952\(88\)90024-5](https://doi.org/10.1016/0013-7952(88)90024-5)
- Gao GR, Gao GY (1980) Microstructures of loess soils in China. *Kexue Tongbao* 25(7): 597-601.
- Giménez RG, de la Villa RV, Martín JAG (2012) Characterization of loess in Central Spain: a microstructural study. *Environ Earth Sci* 65: 2125-2137. <https://doi.org/10.1007/s12665-011-1193-7>
- Gu TF, Wang JD, Wang CX, et al. (2019) Experimental study of the shear strength of soil from the Heifangtai Platform of the Loess Plateau of China. *J Soils Sediments* 19: 3463-3475. <https://doi.org/10.1007/s11368-019-02303-9>
- Houston SL, Houston WN, Spadola DJ (1988) Prediction of field collapse of soils due to wetting. *J Geotech Eng* 114(1): 40-58. [https://doi.org/10.1061/\(ASCE\)0733-9410\(1988\)114:1\(40\)](https://doi.org/10.1061/(ASCE)0733-9410(1988)114:1(40))
- Jiang MJ, Hu HJ, Liu F (2012) Summary of collapsible behaviour of artificially structured loess in oedometer and triaxial wetting tests. *Can Geotech J* 49: 1147-1157. <https://doi.org/info:doi/10.1139/t2012-075>
- Jiang MJ, Li T, Hu HJ, et al. (2014a) DEM analyses of one-dimensional compression and collapse behaviour of unsaturated structural loess. *Comput Geotech* 60: 47-60. <https://doi.org/10.1016/j.compgeo.2014.04.002>
- Jiang MJ, Zhang FG, Hu HJ, et al. (2014b) Structural characterization of natural loess and remolded loess under triaxial tests. *Eng Geol* 181: 249-260. <https://doi.org/10.1016/j.enggeo.2014.07.021>
- Lei XY (1988) The types of loess pores in China and their relationship with collapsibility. *Sci China Chem* 31(11): 1398-1411.
- Li H, Li TL, Li P, et al. (2020) Prediction of loess soil-water characteristic curve by mercury intrusion porosimetry. *J Mt Sci* 17(9): 2203-2213. <https://doi.org/10.1007/s11629-019-5929-2>
- Li P, Vanapalli S, Li TL (2016) Review of collapse triggering mechanism of collapsible soils due to wetting. *J Rock Mech Geotech Eng* 8: 256-274. <https://doi.org/10.1016/j.jrmge.2015.12.002>
- Li P, Xie WL, Pak RYS, et al. (2019a) Microstructural evolution of loess soils from the Loess Plateau of China. *Catena* 173: 276-288. <https://doi.org/10.1016/j.catena.2018.10.006>
- Li XA, Li LC, Song YX, et al. (2019b) Characterization of the

- mechanisms underlying loess collapsibility for land-creation project in Shaanxi Province, China—a study from a micro perspective. *Eng Geol* 249: 77–88. <https://doi.org/10.1016/j.enggeo.2018.12.024>
- Li YR, He SD, Deng XH, et al. (2018) Characterization of macropore structure of Malan loess in NW China based on 3D pipe models constructed by using computed tomography technology. *J Asian Earth Sci* 154: 271–279. <https://doi.org/10.1016/j.jseaes.2017.12.028>
- Lin ZG (1995) Variation in collapsibility and strength of loess with age. In: Derbyshire E et al. (eds.), *Genesis and Properties of Collapsible Soils*. Springer Netherlands. pp 247–265. https://doi.org/10.1007/978-94-011-0097-7_13
- Liu Z, Liu FY, Ma FL et al. (2016) Collapsibility, composition, and microstructure of loess in China. *Can Geotech J* 53(4): 673–686. <https://doi.org/10.1139/cgj-2015-0285>
- Ma Y (2017) Multi Scale Research of Loess Structural Behavior. PhD thesis, Northwest University, Xi'an, China. p 19–20. (In Chinese)
- Mandelbrot BB (1982) *The Fractal Geometry of Nature*. W. H. Freeman and Company. pp 95–190.
- Milodowski AE, Northmore KJ, Kemp SJ, et al. (2015) The mineralogy and fabric of 'Brickearths' (loess) in Kent, UK and their relationship to engineering behaviour. *Bull Eng Geol Environ* 74: 1187. <https://doi.org/10.1007/s10064-014-0694-5>
- Monroy R, Zdravkovic L, Ridley A (2010) Microstructural evolution in compacted London Clay during wetting and loading. *Géotechnique* 60(2): 105–119. <https://doi.org/10.1680/geot.8.P.125>
- Mu QY, Ng CWW, Zhou C, et al. (2018). A new model for capturing void ratio-dependent unfrozen water characteristics curves. *Comput Geotech* 101: 95–9. <https://doi.org/10.1016/j.compegeo.2018.04.019>
- Mu QY, Zhou C, Ng CWW (2020) Compression and wetting induced volumetric behavior of loess: Macro- and micro-investigations. *Transp Geotech* 23: 100345. <https://doi.org/10.1016/j.tgeo.2020.100345>
- Muñoz-Castelblanco JA, Delage P, Pereira JM, et al. (2011) Some aspects of the compression and collapse behavior of an unsaturated natural loess. *Géotechnique Lett* 1(2): 17–22. <https://doi.org/10.1680/geolett.11.00003>
- Ng CWW, Mu QY, Zhou C (2017) Effects of soil structure on the shear behaviour of an unsaturated loess at different suctions and temperatures. *Can Geotech J* 54(2): 270–9. <https://doi.org/10.1139/cgj-2016-0272>
- Nouaouria MS, Guenoud M, Laffi B (2008) Engineering properties of loess in Algeria. *Eng Geol* 99: 85–90. <https://doi.org/10.1016/j.enggeo.2008.01.013>
- Peng JB, Lin HZ, Wang QY, et al. (2014) The critical issues and creative concepts in mitigation research of loess geological hazards. *J Eng Geol* 22(4): 684–691. (In Chinese) <https://doi.org/10.13544/j.cnki.jeg.2014.04.014>
- Peng JB, Wang SK, Wang QY, et al. (2019) Distribution and genetic types of loess landslides in China. *J Asian Earth Sci* 170: 329–350. <https://doi.org/10.1016/j.jseaes.2018.11.015>
- Rogers CDF, Dijkstra TA, Smalley IJ (1994) Hydro-consolidation and subsidence of loess: studies from China, Russia, North America and Europe. *Eng Geol* 37(2): 83–113. [https://doi.org/10.1016/0013-7952\(94\)90045-0](https://doi.org/10.1016/0013-7952(94)90045-0)
- Romero E, Simms PH (2008) Microstructure investigation in unsaturated soils: a review with special attention to contribution of mercury intrusion porosimetry and environmental scanning electron microscopy. *J Geotech Geol Eng* 26(6): 705–727. <https://doi.org/10.1007/s10706-008-9204-5>
- Shao XX, Zhang HY, Tan Y (2018) Collapse behavior and microstructural alteration of remolded loess under graded wetting tests. *Eng Geol* 233: 11–22. <https://doi.org/10.1016/j.enggeo.2017.11.025>
- Standardization Administration of China, Ministry of Housing and Urban-Rural Construction (2018) China National Standards GB50025-2018: Standard for building construction in collapsible loess regions. China Building Industry Press. pp 19. (In Chinese)
- Tadepalli R, Fredlund DG (1991) The collapse behaviour of a compacted soil during inundation. *Can Geotech J* 28(4): 477–488. [https://doi.org/10.1016/0148-9062\(92\)93849-F](https://doi.org/10.1016/0148-9062(92)93849-F)
- Wang JD, Li P, Ma Y, et al. (2020a) Change in pore-size distribution of collapsible loess due to loading and inundating. *Acta Geotech* 15(5): 1081–1094. <https://doi.org/10.1007/s11440-019-00815-9>
- Wang Q, Wang JP (2000) A Study on fractal of porosity in the soils. *Chin J Geotech Eng* 22(4): 496–498. (In Chinese) <https://doi.org/CNKI:SUN:YTGC.0.2000-04-024>
- Wang XG, Wang JD, Zhan HB, et al. (2020b) Moisture content effect on the creep behavior of loess for the catastrophic Baqiao landslide. *Catena* 187: 104371. <https://doi.org/10.1016/j.catena.2019.104371>
- Washburn EW (1921) The dynamics of capillary flow. *Phys Rev* 17(3): 273. <https://doi.org/10.1103/PhysRev.17.273>
- Wei TT, Fan W, Yuan WN et al. (2019) Three-dimensional pore network characterization of loess and paleosol stratigraphy from South Jingyang Plateau, China. *Environ Earth Sci* 78(11): 333. <https://doi.org/10.1007/s12665-019-8331-z>
- Wei YN, Fan W, Yu B et al. (2020) Characterization and evolution of three-dimensional microstructure of Malan loess. *Catena* 192: 104585. <https://doi.org/10.1016/j.catena.2020.104585>
- Xie WL, Li P, Zhang MS, et al. (2018) Collapse behavior and microstructural evolution of loess soils from the Loess Plateau of China. *J Mt Sci* 15(8): 1642–1657. <https://doi.org/10.1007/s11629-018-5006-2>
- Xing YC, Gao DH, Jin SL, et al. (2019) Study on Mechanical Behaviors of Unsaturated Loess in terms of Moistening Level. *KSCE J Civ Eng* 23(3): 1055–1063. <https://doi.org/10.1007/s12205-019-0848-x>
- Xu L, Dai FC, Gong QM, et al. (2012) Irrigation-induced loess flow failure in Heifangtai Platform, North-West China. *Eng Geol* 66(6): 1707–1713. <https://doi.org/10.1007/s12665-011-0950-y>
- Yan RX, Peng JB, Huang QB, et al. (2019) Triggering Influence of Seasonal Agricultural Irrigation on Shallow Loess Landslides on the South Jingyang Plateau, China. *Water* 11: 1474. <https://doi.org/10.3390/w11071474>
- Yang YL (1989) Study of the mechanism of loess collapse. *Sci China, Ser B* 32: 604–617. <https://doi.org/CNKI:SUN:JBXG.0.1989-05-009>
- Yang YS, Li J, Xing YC, et al. (2017) Experimental study on moistening deformation characteristics of compacted loess and their influencing factors. *Chin J Geotech Eng* 39(4): 626–635. (In Chinese) <https://doi.org/10.11779/CJGE201704006>
- Zhang FY, Yan BB, Feng XM, et al. (2019a) A rapid loess mudflow triggered by the check dam failure in a bulldoze mountain area, Lanzhou, China. *Landslides* 16(10): 1981–1992. <https://doi.org/10.1007/s10346-019-01219-2>
- Zhang XZ, Lu YD, Li X, et al. (2019b) Microscopic structure changes of Malan loess after humidification in South Jingyang Plateau, China. *Environ Earth Sci* 78: 287. <https://doi.org/10.1007/s12665-019-8290-4>
- Zhao M, Guo W, Chen LY, et al. (2019) Experiment on the frost resistance of Modified Phospho Gypsum: A case used to Improve Baozhong Railway Subgrade loess. *J Mt Sci* 16(12): 2920–2930. <https://doi.org/10.1007/s11629-018-5014-2>
- Zhu XH, Peng JB, Tong X, et al. (2017) Preliminary research on geological disaster chains in loess area. *J Eng Geol* 25(1): 117–122. (In Chinese) [https://doi.org/1004-9665\(2017\)25:1<117:HTDQDZ>2.0.TX;2-L](https://doi.org/1004-9665(2017)25:1<117:HTDQDZ>2.0.TX;2-L)
- Zhuang JQ, Peng JB, Zhu Y, et al. (2020) The internal erosion process and effects of undisturbed loess due to water infiltration. *Landslides* 18: 629–638. <https://doi.org/10.1007/s10346-020-01518-z>